nature COMMUNICATIONS

ARTICLE

Received 15 May 2014 | Accepted 4 Sep 2014 | Published 10 Oct 2014

DOI: 10.1038/ncomms6155

SLO-2 potassium channel is an important regulator of neurotransmitter release in *Caenorhabditis elegans*

Ping Liu[1], Bojun Chen[1] & Zhao-Wen Wang[1]

Slo2 channels are prominent K^+ channels in mammalian neurons but their physiological functions are not well understood. Here we investigate physiological functions and regulation of the *Caenorhabditis elegans* homologue SLO-2 in motor neurons through electrophysiological analyses of wild-type and mutant worms. We find that SLO-2 is the primary K^+ channel conducting delayed outward current in cholinergic motor neurons, and one of two K^+ channels with this function in GABAergic motor neurons. Loss-of-function mutation of *slo-2* increases the duration and charge transfer rate of spontaneous postsynaptic current bursts at the neuromuscular junction, which are physiological signals used by motor neurons to control muscle cells, without altering postsynaptic receptor sensitivity. SLO-2 activity in motor neurons depends on Ca^{2+} entry through EGL-19, an L-type voltage-gated Ca^{2+} channel (Ca_V1), but not on other proteins implicated in either Ca^{2+} entry or intracellular Ca^{2+} release. Thus, SLO-2 is functionally coupled with Ca_V1 and regulates neurotransmitter release.

[1] Department of Neuroscience, University of Connecticut Health Center, Farmington, Connecticut 06030, USA. Correspondence and requests for materials should be addressed to Z.-W.W. (email: zwwang@uchc.edu).

A major function of K^+ channels in neurons is to regulate the release of neurotransmitters. A variety of K^+ channels have been found to have this physiological function, including the Ca^{2+}- and voltage-gated high-conductance K^+ channel Slo1 (BK channel)[1]. Recent studies show that two other large-conductance K^+ channels of the Slo gene family, Slo2.2 (*Slack*) and Slo2.1/*Slick*, are also broadly expressed in the nervous system[2,3] (www.brain-map.org). Slo2.2 plays major roles in conducting delayed outward current in diverse mammalian central neurons examined[4–6]. Suppression of Slo2.2 expression may enhance neuron excitability and pain sensitivity[7–9]. A strong link has been established between mutations of *KCNT1* (gene encoding Slo2.2) and epileptic disorders[10–14]. These observations suggest that Slo2 channels in neurons may play important physiological roles. However, studies on Slo2 channels with either knockout preparations or specific blockers are lacking, which makes it difficult to precisely define their physiological roles.

Slo2 channels are activated by membrane depolarization and cytosolic Cl^- and Na^+ (refs 15,16). They are considered to be the molecular entity of Na^+-activated K^+ (K_{Na}) channels observed in a variety of cells[17,18]. One conundrum about K_{Na} channels is that a concentration of Na^+ much higher than what could possibly occur in the bulk cytoplasm under physiological conditions is required for significant channel activation[17,18], although these channels appear to be active under physiological conditions[5,19–21]. Recent studies of Slo2.2 suggest that Na^+ entry, through either a persistent tetrodotoxin-sensitive channel(s) of unknown molecular identity[4–6] or AMPA receptors[22], may produce Na^+ microdomains necessary for K_{Na} channel activation.

Caenorhabditis elegans has a single Slo2 orthologue known as SLO-2, which is also gated by voltage and intracellular Cl^- but differs from mammalian Slo2 in that intracellular Ca^{2+} instead of Na^+ activates the channel[23,24]. The $[Ca^{2+}]$ required for *C. elegans* SLO-2 activation[23] is also much higher than what could possibly occur in the bulk cytoplasm under physiological condition. It is unknown whether Ca^{2+} entry plays an analogous role in SLO-2 activation as does Na^+ entry for Slo2 activation. In *C. elegans* body-wall muscle, SLO-2 conducts ~70% of the total delayed outward current, and *slo-2* loss-of-function (*lf*) mutation results in a more depolarized resting membrane potential, a wider action potential waveform and a smaller amplitude of afterhyperpolarization, suggesting that SLO-2 plays important roles in controlling muscle function[25]. Although SLO-2 is also expressed in the nervous system[23,26], its physiological roles in neurons are unknown.

C. elegans neuromuscular junction (NMJ) is often used as a model synapse for analysing the roles of proteins in synaptic transmission. However, electrophysiological analyses of this synapse have been limited to recording postsynaptic current (PSC) from body-wall muscle cells. To our knowledge, there has been no report on whole-cell voltage- and current-clamp recordings from *C. elegans* motor neurons. In the present study, we successfully performed electrophysiological recordings of motor neurons, and combined the electrophysiological data with PSCs recorded from body-wall muscle cells to assess physiological roles of SLO-2 in motor neurons. Our results suggest that SLO-2 is a major contributor to delayed outward current in motor neurons with its activity dependent on Ca^{2+} entry through a L-type voltage-gated Ca^{2+} channel (VGCC), and that SLO-2 controls the strength of synaptic transmission by regulating the duration and charge transfer rate of PSC bursts, which are used by motor neurons to control body-wall muscle[27]. The prominent roles of Slo2/SLO-2 in conducting delayed outward current in both mammalian and nematode neurons suggest that these channels likely have important and conserved physiological functions.

Results

SLO-2 is important to outward current in motor neurons. Motor neurons controlling *C. elegans* body-wall muscle include the following three major classes: A, B and D. The A and B classes mediate backward and forward movements, respectively, and contract muscle by releasing acetylcholine (ACh), whereas the D class relaxes muscle by releasing GABA (γ-aminobutyric acid)[28,29]. To investigate physiological roles of SLO-2 in motor neurons, we chose VA5, VB6 and VD5 (the letter 'V' stands for ventral) as representatives of the three classes of motor neurons because these ventral muscle-innervating neurons could be easily identified based on their anatomical locations (Fig. 1a). We first examined the effect of *slo-2* mutation on delayed outward current in response to voltage steps (-60 to $+70$ mV at 10-mV intervals). The amplitude of delayed outward current was greatly decreased in *slo-2(nf101)*, a putative null resulting from a deletion[30], compared with wild type (WT) in all the motor neurons (Fig. 1b). The decrease was more severe in VA5 and VB6 than VD5. Compared with WT, delayed outward current at $+70$ mV decreased by 80% in VA5 (168.9 ± 16.6 versus 33.6 ± 2.4 pA/pF), 67% in VB6 (176.1 ± 13.4 versus 58.1 ± 3.1 pA/pF) and 33% in VD5 (197.1 ± 12.5 versus 131.9 ± 5.6 pA/pF) (Fig. 1b). The deficiency of delayed outward current in the mutant was rescued by expressing a SLO-2::GFP fusion protein, in which GFP coding sequence was fused in-frame to the 3′-end of *slo-2b* (F08B12.3b) cDNA (www.wormbase.org)[23], under the control of the pan-neuronal *rab-3* promoter (P*rab-3*; refs 31,32; Fig. 1b), suggesting that the deficiency resulted from *slo-2* mutation in neurons, and that the SLO-2::GFP fusion protein was functional.

The persistence of some delayed outward current in *slo-2(nf101)* suggests that there is at least one more K^+ channel functioning in motor neurons. It is difficult to do a comprehensive survey for the many voltage-gated K^+ channels existing in *C. elegans*[33]. Previous studies show that three voltage-gated K^+ channels are important to outward current in *C. elegans* body-wall muscle cells, including SLO-2, SHK-1 (*Shaker* or K_V1) and SHL-1 (*Shal* or K_V4), with SLO-2 and SHK-1 conducting delayed outward current and SHL-1 conducting a fast and transient outward current[25,34,35]. This knowledge was used as a guide in identifying the remaining K^+ channel(s) contributing to outward current in motor neurons. SLO-1, the *C. elegans* Slo1/BK channel, was also included in our analyses because it is expressed in *C. elegans* motor neurons and plays an important role in regulating neurotransmitter release[36]. The mutants analysed included *shk-1(ok1581)*, *shl-1(ok1168)* and *slo-1(md1745)*, which are all putative nulls[25,35,36]. Delayed outward current was normal in VA5 and VB6 of all the mutants (Fig. 1b) but greatly decreased in VD5 of *shk-1(ok1581)* (Fig. 1b). In fact, delayed outward current of VD5 was decreased to a larger degree in *shk-1(ok1581)* (45%) than *slo-2(nf101)* (33%) at $+70$ mV (WT 197.1 ± 12.5 pA/pF; *shk-1* 108.9 ± 15.6 pA/pF; *slo-2* 131.9 ± 5.6 pA/pF) and was essentially absent in the double mutant (Fig. 1b).

Collectively, the aforementioned observations suggest that delayed outward current of VA5 and VB6 results primarily from SLO-2 with a small contribution from an unidentified channel(s), whereas that of VD5 results almost completely from SHK-1 and SLO-2.

SLO-2 regulates membrane potential of motor neurons. In WT worms, the resting membrane potential was -71.7 ± 2.4 mV in VA5, -53.2 ± 2.5 mV in VB6 and -45.8 ± 1.9 mV in VD5. It became significantly less hyperpolarized in *slo-2(nf101)* but was

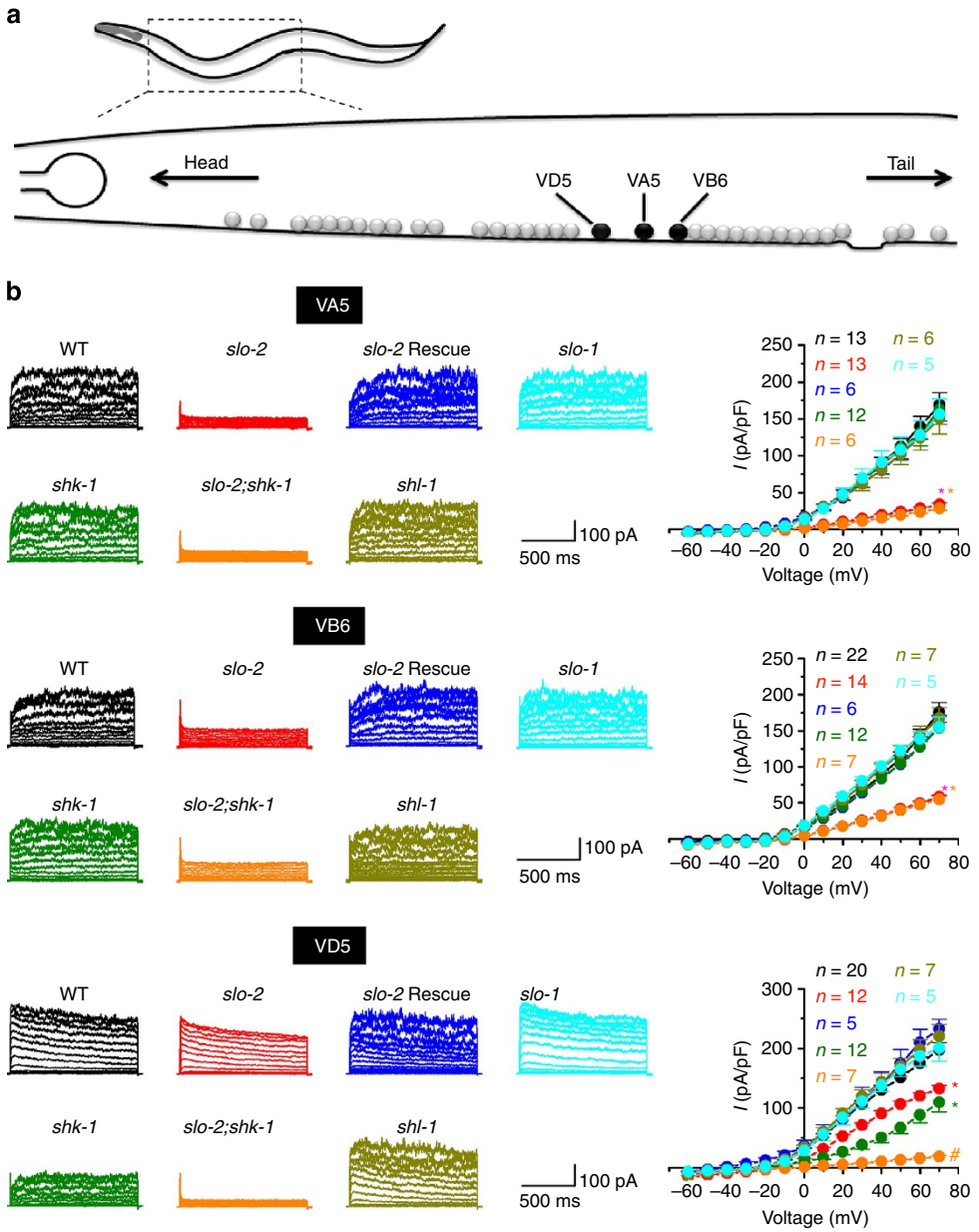

Figure 1 | SLO-2 is an important contributor to delayed outward current in cholinergic and GABAergic motor neurons. (**a**) Diagram showing the locations of the recorded motor neurons VD5, VA5 and VB6 (based on published anatomical data[63]). (**b**) Sample whole-cell current traces in response to voltage steps (− 60 to + 70 mV at 10 mV intervals) from a holding voltage of − 60 mV (left) and current–voltage relationships (right) from VA5, VB6 and VD5 of WT, *slo-2(nf101)*, *slo-2* rescue, *shk-1(ok1581)*, *slo-2(nf101);shk-1(ok1581)*, *shl-1(ok1168)* and *slo-1(md1745)*. In VA5 and VB6, delayed outward current was greatly decreased in *slo-2(nf101)* compared with WT but not further decreased in the *slo-2;shk-1* double mutant. In VD5, delayed outward current was greatly decreased in both *slo-2(nf101)* and *shk-1(ok1581)*, and was essentially absent in the *slo-2;shk-1* double mutant. Data are shown as mean ± s.e. The asterisk (*) indicates a significant difference compared with WT, whereas the pound sign (#) indicates a significant difference compared with the single mutants of *slo-2* and *shk-1* ($P<0.01$, two-way mixed model analyses of variance with Tukey's *post hoc* tests). The recordings were performed with extracellular solution I and pipette solution I.

restored to WT level in the *slo-2(nf101)* strain expressing P*rab-3*::SLO-2::GFP (Table 1). In contrast, mutants of the other K^+ channels did not show a change of the resting membrane potential compared with WT (Table 1). These observations suggest that SLO-2 plays an important role in setting the resting membrane potential of both cholinergic and GABAergic motor neurons.

To assess the role of SLO-2 in regulating motor neuron activity, we analysed spontaneous membrane voltage changes of VA5. In both WT and *slo-2(nf101)*, the membrane voltage alternated between the resting membrane potential and an upstate, with apparent spontaneous postsynaptic potentials decorating both periods (Fig. 2a). The upstate often reached a similar level in each recording and never overshot (Fig. 2a). Compared with WT, the upstate of *slo-2(nf101)* was 61% smaller in amplitude (33.4 ± 1.4 versus 13.1 ± 0.9 mV) and 45% longer in duration (14.9 ± 1.5 versus 21.6 ± 2.6 s) without a change in frequency (Fig. 2b). Since upstate potential (the mean membrane potential during the upstate) was similar between WT and *slo-2(nf101)* (Fig. 2b), the smaller upstate amplitude of the mutant resulted from the elevated resting membrane potential.

Table 1 | Comparison of the resting membrane potential of motor neurons between wild type and K^+ channel mutants.

Genotype	VA5	VB6	VD5
Wild type	−71.7 ± 2.4 (*n* = 15)	−53.2 ± 2.5 (*n* = 13)	−45.8 ± 1.9 (*n* = 15)
slo-2	−46.5 ± 2.0 (*n* = 12)*	−24.0 ± 3.3 (*n* = 8)*	−25.2 ± 1.6 (*n* = 12)*
slo-2 Rescue	−71.5 ± 2.2 (*n* = 8)	−48.3 ± 2.1 (*n* = 6)	−48.2 ± 2.5 (*n* = 7)
shk-1	−67.9 ± 3.9 (*n* = 11)	−51.3 ± 2.4 (*n* = 9)	−42.6 ± 3.2 (*n* = 6)
slo-2;shk-1	−43.9 ± 2.8 (*n* = 9)*	−19.9 ± 1.1 (*n* = 7)*	−20.3 ± 2.4 (*n* = 6)*
shl-1	−68.0 ± 3.6 (*n* = 7)	−50.0 ± 3.9 (*n* = 7)	−48.7 ± 2.6 (*n* = 5)
slo-1	−69.0 ± 3.0 (*n* = 9)	−54.9 ± 2.8 (*n* = 7)	−46.1 ± 2.6 (*n* = 7)

Data are shown as mean ± s.e. Asterisk (*) indicates a statistically significant difference compared with wild type ($P < 0.01$, one-way analyses of variance with Tukey's *post hoc* test).

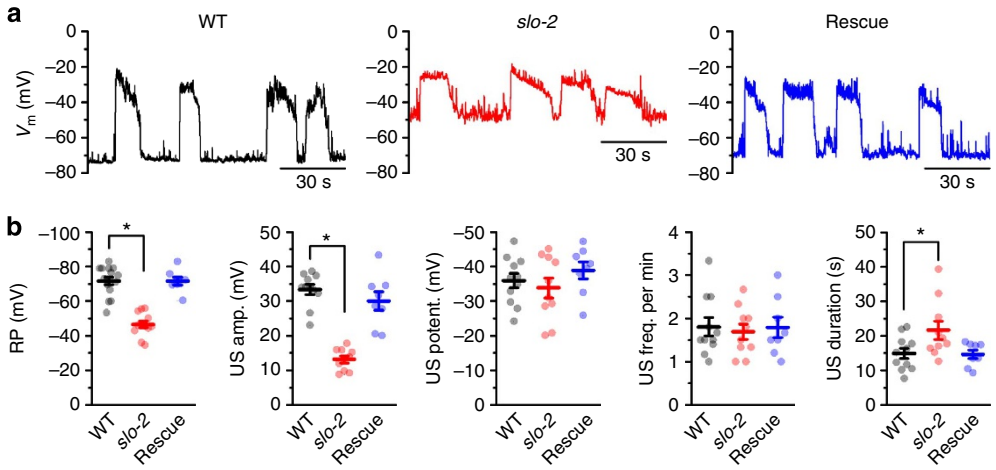

Figure 2 | Loss-of-function mutation of *slo-2* reduced the amplitude of a spontaneous upstate in motor neurons. (**a**) Samples traces of spontaneous membrane voltage changes of VA5 from wild type (WT), *slo-2(nf101)* and *slo-2(nf101)* rescued by expressing WT SLO-2b under the control of P*rab-3*. (**b**) Comparison of the resting membrane potential (RP) and upstate (US) frequency (freq.), duration, amplitude (amp.) and potential (potent.). Both the averaged value of each experiment (filled circle) and the mean ± s.e. of the group (line and bar) are shown. The asterisk (*) indicates a statistically significant difference compared with WT ($P < 0.05$, one-way analyses of variance with Tukey's *post hoc* tests). The sample size (*n*) was 15 for WT, 12 for *slo-2* and 8 for Rescue. Samples without obvious USs (four WT and two *slo-2* mutant) were not included in the US quantifications. The recordings were performed with extracellular solution I and pipette solution I.

SLO-2 regulates neurotransmitter release. To determine whether SLO-2 in motor neurons regulates synaptic transmission, we analysed spontaneous and evoked PSCs at the *C. elegans* NMJ. We first focused on spontaneous PSC bursts, defined as an apparent increase in PSC frequency with a persistent current lasting >3 s, because they are the physiological signals used by motor neurons to control muscle contractility[27]. The persistent current, appearing as an apparent downward shift of the baseline, was used to demarcate PSC bursts, as described previously[27]. Cholinergic PSC bursts were isolated by using pipette and extracellular solutions with the Cl^- equilibrium potential equal to the holding potential (−60 mV). Compared with WT, *slo-2(nf101)* showed significantly longer duration and higher charge transfer rate in PSC bursts, which were restored to WT level when SLO-2::GFP was expressed in neurons (Fig. 3a,b). The main cause for the higher charge transfer rate of PSC bursts in *slo-2(nf101)* was a larger mean persistent current because amplitude of the persistent current increased by 87% (WT 4.6 ± 0.5 pA; *slo-2* 8.6 ± 0.8 pA) (Fig. 3b) but frequency and amplitude of intra-burst PSC events were unaltered compared with WT (Fig. 3c).

The larger persistent current of cholinergic PSC bursts observed in *slo-2(nf101)* could have resulted from either increased neurotransmitter release or increased postsynaptic receptor sensitivity to ACh. To examine the second possibility, we compared the amplitude of inward current caused by pressure-ejecting exogenous ACh (100 μM) to body-wall muscle cells between WT and *slo-2(nf101)*. A similar experiment with exogenous GABA (100 μM) was also performed although GABA did not contribute to the PSC bursts under the experimental conditions[27]. We found that amplitudes of ACh- and GABA-induced inward current were similar between WT and *slo-2(nf101)* (Fig. 4a). Thus, the larger persistent current of PSC bursts in *slo-2(nf101)* did not result from an increased postsynaptic receptor function or expression.

We also compared evoked PSCs (ePSCs) caused by electric stimulation of motor neurons between WT and *slo-2(nf101)*. Evoked PSCs were analysed in the presence of two different $[Ca^{2+}]_o$ (5 and 0.5 mM) because an effect of *slo-2* mutation on the evoked responses could potentially vary depending on $[Ca^{2+}]_o$, as is the case with *slo-1* mutation[37]. We found that evoked PSCs were similar in amplitude between WT and *slo-2(lf)* in the presence of either 5 or 0.5 mM $[Ca^{2+}]_o$ (Fig. 4b), suggesting that SLO-2 does not regulate neurotransmitter release caused by strong non-physiological stimuli.

SLO-2 in motor neurons requires Cl^- and Ca^{2+} for activation. Analyses with inside-out patches from *Xenopus* oocytes show that SLO-2 has a mean single-channel conductance of 110 pS in symmetrical K^+, and is activated synergistically by Ca^{2+} and Cl^- on the intracellular side[23]. However, single-channel conductance of SLO-2 in neurons has not been reported,

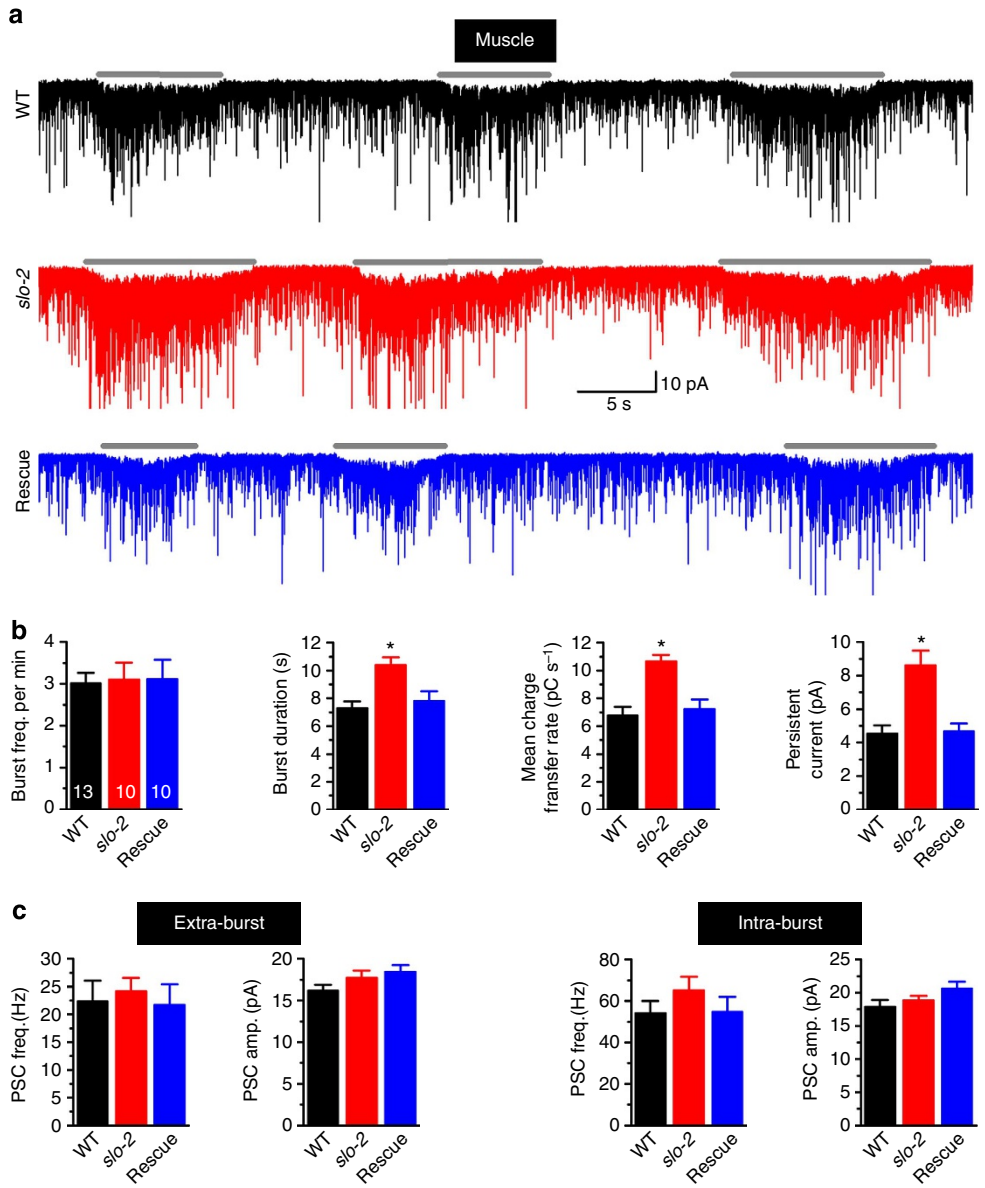

Figure 3 | SLO-2 deficiency augmented PSC bursts recorded from body-wall muscle. (**a**) Representative traces of spontaneous PSC. The horizontal grey line marks PSC bursts. (**b**) Comparison of PSC burst properties. (**c**) Comparison of extra- and intra-burst PSC events. The sample sizes (*n*) were 17 for wild type (WT), 15 for *slo-2*(*nf101*) and 10 for *slo-2*(*nf101*) expressing P*rab-3*::SLO-2::GFP (Rescue). Data are shown as mean ± s.e. The asterisk (*) indicates a statistically significant difference compared with WT ($P<0.05$, one-way analyses of variance with Tukey's *post hoc* tests). The recordings were performed with extracellular solution I and pipette solution II. Amp., amplitude; freq., frequency.

the concentration of free Ca^{2+} required for significant SLO-2 activity[23] is much higher than what could possibly be reached in the bulk cytoplasm under physiological conditions, and the reported Cl^- sensitivity of SLO-2 was rebutted by a recent study[38]. We therefore performed experiments to assess the single-channel conductance of SLO-2 in motor neurons and to determine whether SLO-2 in motor neurons is sensitive to Ca^{2+} and Cl^-. First, we recorded SLO-2 single-channel activities in inside-out patches held at a series of voltages in the presence of symmetrical K^+ solutions to determine SLO-2 single-channel conductance. In WT, each patch typically showed activities of a few channels, which were apparently of the same type (Fig. 5a). In contrast, similar single-channel opening events were never observed in *slo-2(lf)* (Fig. 5a). We determined SLO-2 single-channel conductance from the slope of a linear fit to SLO-2 single-channel current amplitudes at the various voltages, and found it to be 117 ± 2 pS in VA5, 120 ± 2 pS in VB6 and 111 ± 2 pS in VD5 (Fig. 5b). These values are similar to those of SLO-2 expressed in *Xenopus* oocytes[23] and in cultured body-wall muscle cells[34]. Next, we analysed the effect of intracellular Cl^- on SLO-2 by reducing $[Cl^-]$ from 128.5 to 15.3 mM in the standard pipette solution. This treatment essentially abolished SLO-2 current in WT worms, as suggested by the similar outward current between WT with low $[Cl^-]_i$ and *slo-2(lf)* with high $[Cl^-]_i$, and the lack of an effect of the low $[Cl^-]_i$ on outward current in *slo-2(lf)* (Fig. 6a). Finally, we analysed SLO-2 Ca^{2+} dependence. In recording the whole-cell current, the concentration of free Ca^{2+} in the pipette solution was ~50 nM, which was not expected to cause significant SLO-2 activation[23]. We hypothesized that extracellular Ca^{2+} plays a role in SLO-2 activation by establishing Ca^{2+} microdomains at the inner openings of Ca^{2+} permeable channels, as is the case for

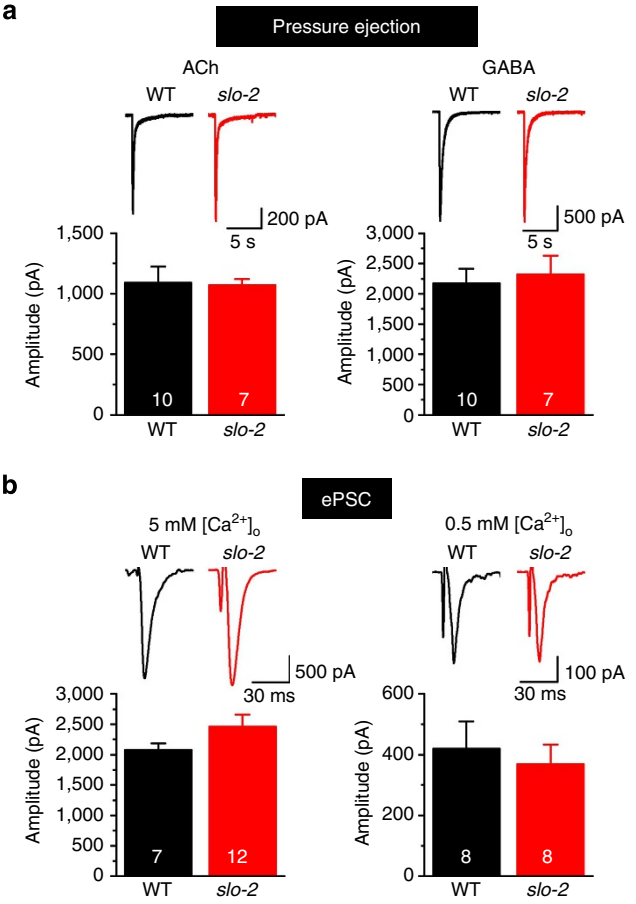

Figure 4 | Postsynaptic receptor sensitivities and evoked postsynaptic currents (ePSCs) were normal in *slo-2(nf101)*. (**a**) Comparison of muscle cell response to pressure-ejected acetylcholine (ACh; 100 μM) or GABA (100 μM) between wild type (WT) and *slo-2(nf101)*. (**b**) Comparison of ePSC between WT and *slo-2(nf101)* in the presence of two different extracellular Ca^{2+} concentrations (5 and 0.5 mM). Data are shown as mean ± s.e. No significant difference was detected (unpaired *t*-test). The holding voltage was −60 mV in all the experiments. The numbers inside the columns indicate the sample sizes (*n*). All the recordings were performed with pipette solution I. The recordings of ePSC at 0.5 mM $[Ca^{2+}]_o$ were performed with extracellular solution II, whereas the remaining recordings were recorded with extracellular solution I.

mammalian Slo2 activation by extracellular Na^+ (refs 4,5). We therefore examined the effects of varying $[Ca^{2+}]_o$ between 5 and 0 mM on SLO-2 single-channel activity in outside-out patches with little free Ca^{2+} (~50 nM) in the pipette solution. Indeed, SLO-2 activity was high when $[Ca^{2+}]_o$ was 5 mM but greatly decreased after $[Ca^{2+}]_o$ was changed to 0 mM (Fig. 6b). Taken together, our observations suggest that SLO-2 in motor neurons depends on both Cl^- and Ca^{2+} for activation, and that extracellular Ca^{2+} plays an important role in SLO-2 activation.

Ca^{2+} entry through EGL-19 is important to SLO-2 activation. Given that SLO-2 was activated by Ca^{2+} entering the cell, there must be a Ca^{2+} channel(s) mediating the Ca^{2+} entry. We first examined potential contributions by VGCCs. The *C. elegans* genome contains three genes encoding the pore-forming α_1-subunit of VGCCs, including *egl-19* (Ca_V1/L-type), *unc-2* (Ca_V2/N, P, Q-type) and *cca-1* (Ca_V3/T-type)[39]. We selected mutants of these genes for analyses. For *unc-2* and *cca-1*, we analysed the severe *lf* or null mutants *unc-2(e55)* and *cca-1(ad1650)* (refs 40,41). For *egl-19*, we analysed the gain-of-function mutant *egl-19(ad695)* and the hypomorphic mutant *egl-19(n582)* because null mutants die at embryonic stages[42]. Compared with WT, *egl-19(ad695)* caused a significantly larger delayed outward current in all the motor neurons (VA5, VB6 and VD5), whereas *egl-19(n582)* showed an opposite effect in VA5 and VB6 (Fig. 7). These effects of the *egl-19* mutants were not observed in the presence of *slo-2(nf101)* (Fig. 7), suggesting that EGL-19 regulates delayed outward current through SLO-2. The insignificant effect of *egl-19(n582)* on delayed outward current in VD5 (Fig. 7) could be owing to the relatively small SLO-2 current in VD5 (Fig. 1).

Delayed outward current was similar between WT and either *unc-2(e55)* or *cca-1(ad1650)* (Fig. 8), suggesting that UNC-2 and CCA-1 do not play a role in SLO-2 activation. In addition to the VGCCs, we assessed potential contributions by several other proteins implicated in either Ca^{2+} entry or Ca^{2+} release from endoplasmic reticulum, including TRP-1 (canonical transient receptor potential channel)[43], CLHM-1 (calcium homeostasis modulator, Calhm)[44], NCA-1 and NCA-2 (putative cation channels)[45,46], and UNC-68 (ryanodine receptor)[47,48] by analysing whole-cell current in corresponding mutants. The mutant strains used included *trp-1(ok323)* (refs 49,50), *clhm-1(ok3617)* (ref. 44), *unc-68(r1162)* (ref. 47) and the double-mutant *nca-1(gk9);nca-2(gk5)* (refs 45,46,51), which are either nulls or severe *lf* mutants. Delayed outward current was normal in all these mutants (Fig. 8). Taken together, the aforementioned observations suggest that EGL-19 is likely the primary, if not the only, Ca^{2+} channel mediating SLO-2 activation in motor neurons.

Discussion

Our electrophysiological data indicate that SLO-2 is the primary contributor to delayed outward current in A and B class motor neurons, and one of two major contributors to this current in D class motor neurons. These observations are reminiscent of those with rat central neurons where Slo2 channels contribute to a large portion of delayed outward current[4–6]. The similar observations with rat and *C. elegans* suggest that these channels began to assume the important task of conducting delayed outward current early in evolution, and that their existence has been indispensable.

The resting membrane potential of mammalian neurons is generally close to the K^+ equilibrium potential owing to the function of background K^+ channels. Two-pore domain K^+ (K2P) channels appear to be important molecular entities of the background K^+ channels because they are largely voltage independent[52]. The *C. elegans* genome has 46 K2P genes[33]. Although no experimental evidence is currently available, it is conceivable that some of these channels may play roles in setting the resting membrane potential. The present study shows that SLO-2, which is not a K2P channel, plays an important role in setting the resting membrane potential of motor neurons. A similar role of SLO-2 has been observed in *C. elegans* body-wall muscle[25]. Thus, SLO-2 might be important in setting the resting membrane potential of many *C. elegans* neurons and muscle cells.

slo-2 mutation resulted in a longer duration and a larger persistent current of PSC bursts compared with WT, suggesting that a physiological function of SLO-2 is to shorten the duration and decrease the charge transfer rate of PSC bursts. SLO-2 likely performs these physiological functions by regulating neurotransmitter release because body-wall muscle sensitivities to neurotransmitters are normal in *slo-2* mutant. Given that PSC bursts are the physiological signals used by motor neurons to control body-wall muscle cells[27], SLO-2 likely plays an important role in regulating muscle function. This physiological function of SLO-2

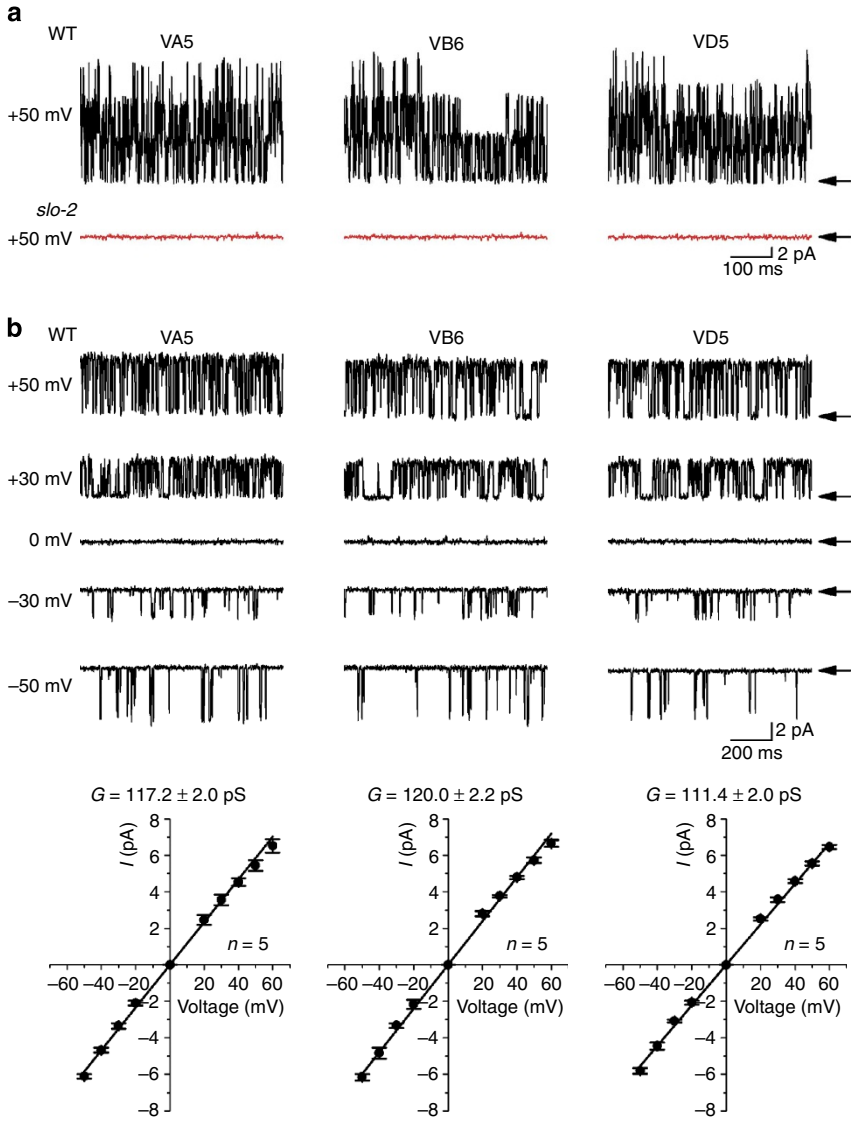

Figure 5 | Single-channel conductance of motor neuron SLO-2. (**a**) Sample current traces showing SLO-2 single-channel activities in inside-out patches of wild type and the absence of such activities in *slo-2(nf101)*. (**b**) Sample SLO-2 single-channel current traces at various membrane voltages from inside-out patches, and the relationship between single-channel current amplitude and holding potential. Data are shown as mean ± s.e. SLO-2 single-channel conductance (*G*) and sample size (*n*) are shown in the graphs. For display purpose, the sample traces were chosen from regions where only one channel was open. Arrows mark the baseline. The experiments were performed in symmetrical K^+ (pipette solution III and bath solution as specified in Methods).

could be related to its effect on the resting membrane potential of motor neurons and its interactions with other proteins such as EGL-19.

The substantial decrease of SLO-2 single-channel activity in outside-out patches following the removal of Ca^{2+} on the extracellular side suggests that SLO-2 activity depends on Ca^{2+} entry. EGL-19 appeared to play an important role in SLO-2 activation as SLO-2 current was significantly increased in *egl-19(gf)* but decreased in *egl-19(hypomorph)*. Indeed, EGL-19 might be the only channel with this function given that mutants of a variety of other genes known to be important to either entry of extracellular Ca^{2+} or release of Ca^{2+} from the endoplasmic reticulum did not show a change of SLO-2 current. The coupling of SLO-2 activation to Ca^{2+} entry through EGL-19 explains why large SLO-2 current is observed in *C. elegans* motor neurons in whole-cell voltage-clamp experiments with little free Ca^{2+} in the pipette solution. The dependence of SLO-2 activity on EGL-19 is analogous to that of mammalian Slo2 on tetrodotoxin-sensitive Na^+ channels[4,5]. *C. elegans* does not have any genes encoding voltage-gated Na^+ channels and likely uses Ca^{2+} exclusively for carrying excitatory inward current[39], which is in contrast to mammals in which Na^+ action potentials generally underlie cellular excitability. It thus appears that coupling channel activation to the entry of a cation is a conserved property of SLO-2/Slo2 channels, but evolution has tuned this property to match the dominant ion used in cellular excitation in each species.

The *C. elegans* Slo family of K^+ channels includes two members: SLO-1 and SLO-2 (refs 24,33). *slo-1(lf)* also prolongs the duration of PSC bursts[27]. However, there are major differences in synaptic phenotypes between *slo-1* and *slo-2* mutants. Unlike *slo-2(lf)*, *slo-1(lf)* does not alter the persistent current of PSC bursts but may cause larger evoked PSC amplitude at the *C. elegans* NMJ compared with WT[27,37,53]. Thus, SLO-1 and SLO-2 likely inhibit neurotransmitter release through somewhat different mechanisms, which could be related to their different subcellular localization and/or functional coupling to

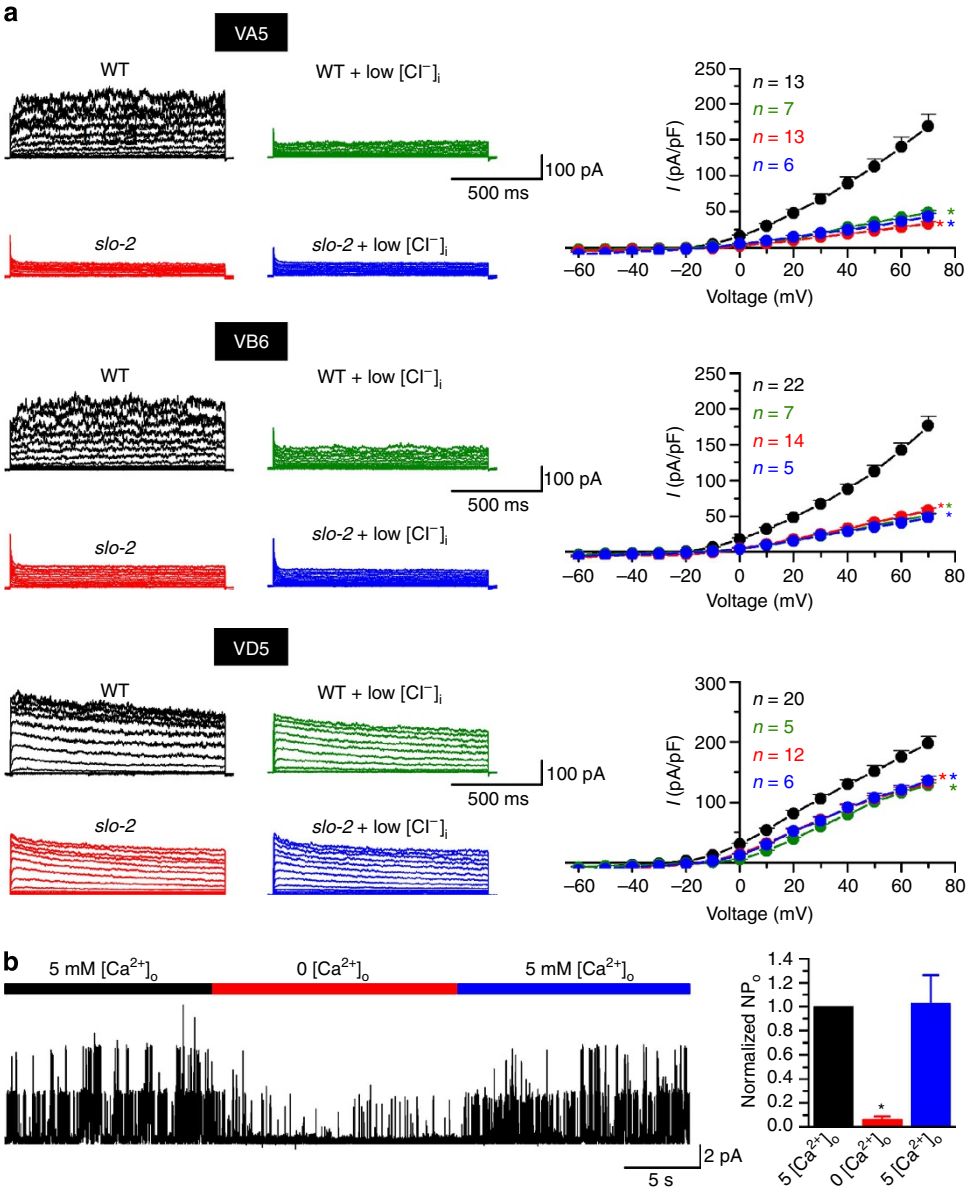

Figure 6 | SLO-2 activity in motor neurons depends on cytosolic [Cl$^-$] and entry of extracellular Ca^{2+}. (**a**) Whole-cell current traces and relationships between delayed outward current and voltage in representative motor neurons (VA5, VB6 and VD5) of wild type (WT), *slo-2(nf101)*, WT with low [Cl$^-$] in pipette solution (WT + low [Cl$^-$]$_i$) and *slo-2(nf101)* with low [Cl$^-$] in pipette solution (*slo-2* + low [Cl$^-$]$_i$), showing that reducing [Cl$^-$]$_i$ from the control level (128.5 mM) to a low level (15.3 mM) caused a great reduction of delayed outward current in WT but no change in *slo-2(nf101)*. The asterisk (*) on the right side of a current–voltage relationship indicates a statistically significant ($P<0.01$) difference compared with WT (two-way mixed model analyses of variance (ANOVA) with Tukey's *post hoc* test). All the recordings were performed with extracellular solution I and pipette solution I except for the low [Cl$^-$] experiments, in which pipette solution II was used instead. (**b**) Effects of varying [Ca^{2+}]$_o$ on SLO-2 single-channel activity in outside-out patches at a holding voltage of +30 mV. The open probability (NP$_o$) of SLO-2 was normalized to that of the first 5 mM [Ca^{2+}]$_o$ period. The asterisk (*) indicates a statistically significant difference compared with the first 5 mM [Ca^{2+}]$_o$ period ($P<0.01$, one-way ANOVA with Tukey's *post hoc* test, $n=5$). The recordings were performed with pipette solution I and either extracellular solution I (5 mM Ca^{2+}) or extracellular solution III (0 Ca^{2+}). In both **a**,**b**, data are shown as mean ± s.e.

different VGCCs. While SLO-1 is localized at the presynaptic site[53] and is likely regulated by Ca^{2+} entry through UNC-2, which is also localized at the presynaptic site[54], SLO-2 might be localized to other subcellular domains and coupled to Ca^{2+} entry through EGL-19.

SLO-1 did not show a detectable contribution to the whole-cell current of motor neurons in spite of its important role in regulating neurotransmitter release. There are two possible causes for this discrepancy. First, the free [Ca^{2+}] of the recording pipette (~50 nM) was insufficient to allow significant SLO-1 activation. Second, SLO-1 current at presynaptic sites, which could potentially result from a coupling to Ca^{2+} entry through UNC-2, might have been shunted before reaching the soma. We have noted a similar discrepancy between SLO-1 function and its contribution to whole-cell current in *C. elegans* body-wall muscle, where SLO-1 is expressed[36] and plays an important role in regulating Ca^{2+} transients[53], but whole-cell current was indistinguishable between WT and *slo-1* null mutant even when a pipette solution containing 20 μM free Ca^{2+} concentration was used in the recording (unpublished observation).

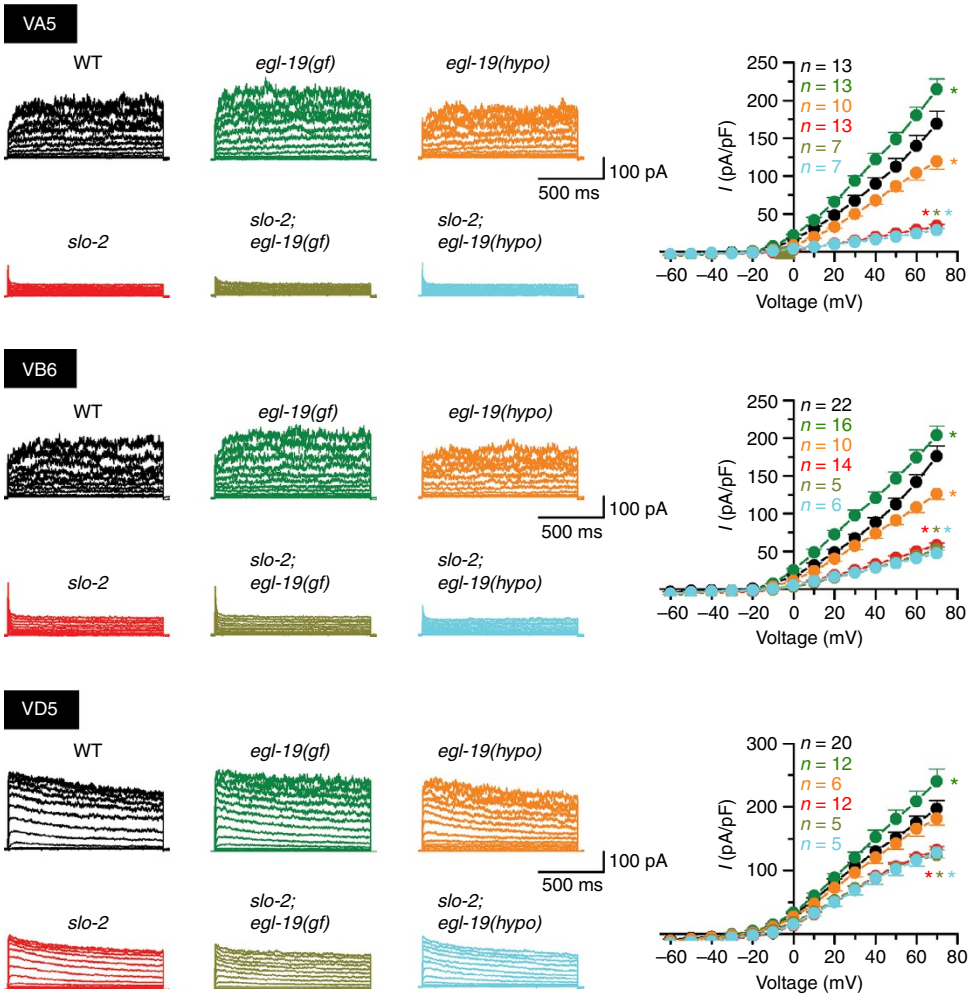

Figure 7 | Mutations of *egl-19* altered delayed outward current of motor neurons in a SLO-2-dependent manner. Whole-cell delayed outward current were recorded from VA5, VB6 and VD5 of wild type (WT), *egl-19(ad695)* (gain-of-function), *egl-19(n582)* (hypomorph), *slo-2(nf101)*, *slo-2(nf101);egl-19(ad695);* and *slo-2(nf101);egl-19(n582)*. Compared with WT, *egl-19(ad695)* and *egl-19(n582)* augmented and inhibited delayed outward current, respectively, which were not observed in the presence of *slo-2(nf101)*. Left: sample current traces in response to voltage steps (− 60 to + 70 mV at 10 mV intervals) from a holding potential of − 60 mV. Right: current–voltage relationships. Data are shown as mean ± s.e. The asterisk (*) indicates a statistically significant difference compared with WT ($P<0.05$, two-way mixed model analyses of variance and Tukey's *post hoc* tests). The recordings were performed with extracellular solution I and pipette solution I.

slo-2 mutant worms displayed no obvious locomotion defects, which is somewhat surprising given that SLO-2 is an important K^+ channel in both body-wall muscle cells[15,25,34] and motor neurons. This is analogous to the movement phenotypes of *slo-1* mutants. Although SLO-1 also plays important physiological roles in both neurons[36,55] and body-wall muscle cells[56–58], *slo-1* mutants only show a slightly larger head bending angle compared with WT, which results from SLO-1 deficiency in body-wall muscle cells, and may be detected only by either a trained observer or computer-based analyses[59,60]. Perhaps potential effects of SLO-2 deficiency on behavioural phenotypes would become more obvious in a sensitized genetic background or under some specific conditions such as hypoxia[15].

The original paper on SLO-2 reported that SLO-2 heterologously expressed in *Xenopus* oocytes is activated by Cl^- on the intracellular side[23]. Consistently, the concentration of Cl^- in the recording pipette solution was found to have a large effect on SLO-2 activity of *C. elegans* body-wall muscle cells *in situ*[34]. However, the Cl^- dependence of SLO-2 was challenged by a recent study showing that at least two isoforms of SLO-2, including the original one used in the heterologous expression experiments, are Cl^- insensitive[38]. It was suggested that the apparent Cl^- dependence of SLO-2 observed in the earlier study reflected contamination by an endogenous Cl^- current present in *Xenopus* oocytes[38]. Our observations provide evidence that SLO-2 in native motor neurons is a Cl^--sensitive channel.

Both the human genome and *C. elegans* genome contain over 70 potassium channel genes[33,61]. The fact that SLO-2/Slo2 channels play a major role in conducting delayed outward current in neurons of both species suggests that this subfamily of K^+ channels likely performs conserved physiological functions of unusual importance. It will be interesting to know whether mammalian Slo2 channels also control the resting membrane potential and regulate synaptic transmission, and how their physiological functions are modulated *in vivo*. Since knockout mice of both Slo2 genes (*KCNT1* and *KCNT2*) are now available from the Jackson laboratory (MGI:1924627 and 3036273), it is desirable to compare between WT and the knockout mice the resting membrane potential and PSCs in selected central neurons. In addition, many Slo2 mutations identified in human epileptic patients may be introduced into worm SLO-2 to investigate how these mutations affect channel function and/or expression *in vivo*.

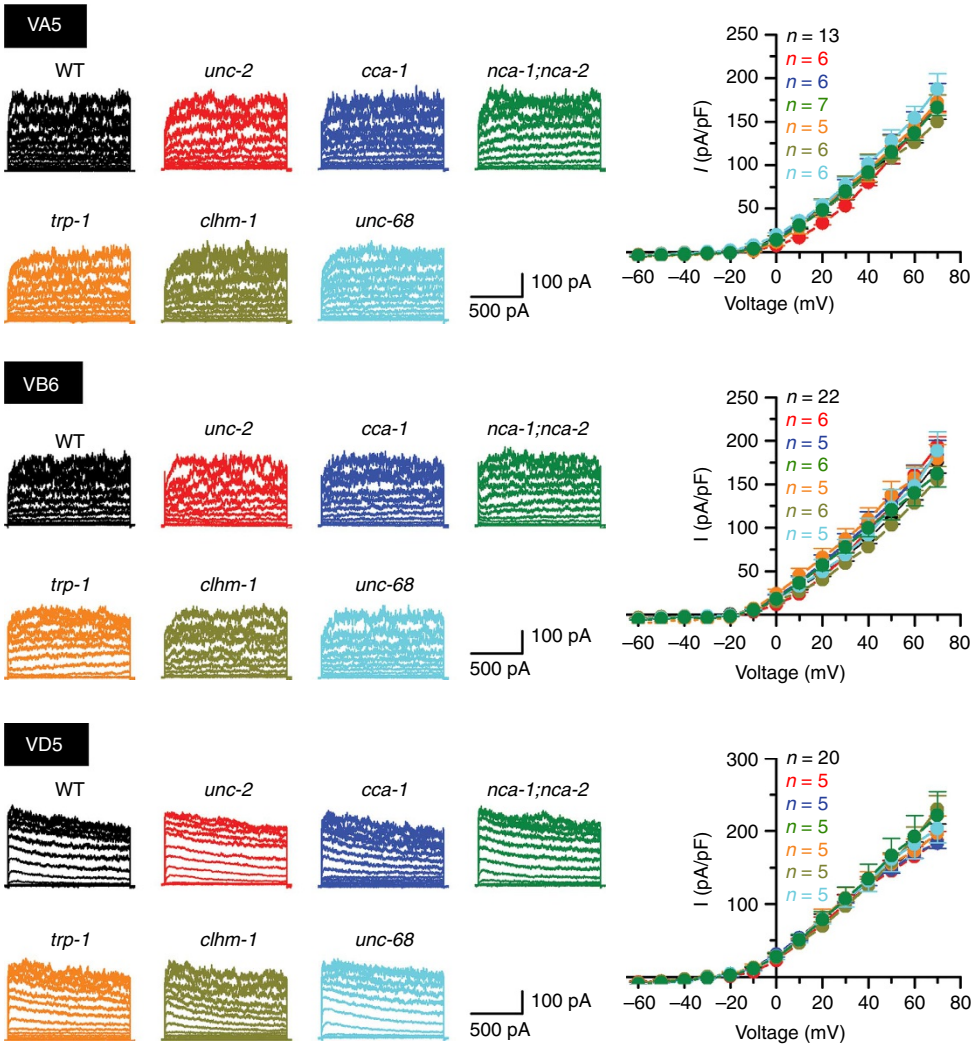

Figure 8 | Delayed outward current was normal in mutants of other Ca^{2+} channels. Delayed outward currents were unchanged in *unc-2(e55)*, *cca-1(ad1650)*, *trp-1(ok323)*, *clhm-1(ok3617)*, *unc-68(r1162)* and the double-mutant *nca-1(gk9);nca-2(gk5)* compared with wild type (WT; two-way mixed model analyses of variance). Left: sample current traces in response to voltage steps (-60 to $+70$ mV at 10 mV intervals) from a holding potential of -60 mV. Right: current–voltage relationships. Data are shown as mean ± s.e. The recordings were performed with extracellular solution I and pipette solution I.

In some cases, expression of a mutated channel may cause an obvious behavioural phenotype, which could serve as a very useful tool for identifying conserved Slo2 channel regulatory proteins through mutant screen in this genetically tractable model organism.

Methods

***C. elegans* culture and strains.** *C. elegans* hermaphrodites were raised on nematode growth medium plates spotted with a layer of OP50 *Escherichia coli* at 21 °C inside an environmental chamber. The strains used included WT (Bristol N2), *slo-2(nf101)*, *shk-1(ok1581)*, *shl-1(ok1168)*, *slo-1(md1745)*, *egl-19(ad695)*, *egl-19(n582)*, *unc-2(e55)*, *cca-1(ad1650)*, *nca-1(gk9);nca-2(gk5)*, *trp-1(ok323)*, *clhm-1(ok3617)*, *unc-68(r1162)*, *slo-2(nf101);shk-1(ok1581)*, *slo-2(nf101);egl-19(ad695)* and *slo-2(nf101);egl-19(n582)*.

Mutant rescue. Neuron-specific rescue was performed by injecting a plasmid containing the pan-neuronal P*rab-3* and full-length *slo-2b* cDNA (F08B12.3b; www.wormbase.org)[23] fused in-frame at its 3′-end to GFP coding sequence into *slo-2(nf101)* using a standard technique[62].

Electrophysiology. All electrophysiological experiments were performed with adult hermaphrodites. An animal was immobilized on a glass coverslip by applying Vetbond^{M} Tissue Adhesive (3M Company, St Paul, MN, USA). Application of the glue was generally restricted to the dorsal anterior portion (excluding the head) of the animal, allowing the head and tail to sway freely during the experiment. A short (~300 μm) longitudinal incision was made along the glued region. After clearing the viscera by suction through a glass pipette, the cuticle flap was folded back and glued to the coverslip, thereby exposing several ventral body-wall muscle cells and a small number of motor neurons anterior to the vulva. Borosilicate glass pipettes were used as electrodes for recording whole-cell and single-channel currents. Pipette tip resistance for recording muscle cell current was 3–5 MΩ, whereas that for recording motor neuron current was ~20 MΩ. The dissected worm preparation was treated briefly with collagenase A (0.5 mg ml^{-1} for 10–15 s; Roche Applied Science, catalogue number 10103578001) and perfused with the extracellular solution for 5- to 10-fold of bath volume. Classical whole-cell configuration was obtained by applying a negative pressure to the recording pipette. Inside-out patches were obtained by quickly pulling away the recording pipette after the formation of a gigaohm seal, whereas outside-out patches were obtained by slowly pulling away the recording pipette after achieving the whole-cell configuration. Current- and voltage-clamp experiments were performed with a Multiclamp 700B amplifier (Molecular Devices, Sunnyvale, CA, USA) and the Clampex software (version 10, Molecular Devices). Data were sampled at a rate of 10 kHz after filtering at 2 kHz. Spontaneous membrane potential changes were recorded using the current-clamp technique without current injection. Motor neuron whole-cell outward currents were recorded by applying a series of voltage steps (-60 to $+70$ mV at 10-mV intervals, 1,200 ms pulse duration) from a holding potential of -60 mV. Evoked PSC, spontaneous PSC and exogenous ACh- or GABA-induced PSC were recorded from body-wall muscle cells at a holding potential of -60 mV. Evoked PSC was caused by applying an electric stimulus at a saturating strength (20 V, 0.5 ms) through a glass pipette electrode placed near the ventral nerve cord. The stimulus was generated by a square pulse stimulator (S48, Grass Technologies, Warwick, RI, USA). To obtain representative evoked PSC from each preparation, the position of the electrode was adjusted until a maximal evoked PSC peak

amplitude was observed. Muscle responses to exogenous ACh and GABA were caused by puffing the chemicals (100 μM) through a glass pipette using a FemtoJet injector (Eppendorf) with the pressure pulse set at 0.2 p.s.i. and 0.1 s.

Solutions. Three different extracellular solutions and three different pipette solutions were used, as specified in figure legends. Extracellular solution I contained (in mM) 140 NaCl, 5 KCl, 5 $CaCl_2$, 5 $MgCl_2$, 11 dextrose and 5 HEPES (pH 7.2). Extracellular solution II differed from extracellular solution I in that $CaCl_2$ was reduced to 0.5 mM. Extracellular solution III differed from extracellular solution I in that $CaCl_2$ was eliminated, 5 mM EGTA was added and NaCl was increased to 150 mM. Pipette solution I contained (in mM) 120 KCl, 20 KOH, 5 Tris, 0.25 $CaCl_2$, 4 $MgCl_2$, 36 sucrose, 5 EGTA and 4 Na_2ATP (pH 7.2). Pipette solution II differed from pipette solution I in that 113.2 KCl was substituted by K^+ gluconate. Pipette solution III contained (in mM) 150 K^+ gluconate, 1 Mg^{2+} gluconate and 10 HEPES (pH 7.2). The bath solution used in inside-out patch experiments contained (in mM) 100 K^+ gluconate, 50 KCl, 1 Mg^{2+} gluconate, 0.1 Ca^{2+} gluconate and 10 HEPES (pH 7.2).

Data analyses. Amplitudes of whole-cell current in response to voltage steps were determined from the mean current during the last 100 ms of the 1,200-ms voltage pulses using the Clampfit software (version 10, Molecular Devices). SPSS software (IBM Corp., New York, USA) was used for comparing the current among different genotypes by two-way mixed model analyses of variance. In these analyses, voltage steps were treated as within-subject variables, whereas genotypes as between-subject variables. Tukey's *post hoc* tests were used to determine whether a statistically significant difference exists between specified genotypes. All genotypes shown inFigs 1 and 6–8 were analysed together so that valid statistical comparisons could be made among them.

SLO-2 single-channel amplitude and open probability were quantified using Clampfit. PSC bursts were identified as an apparent increase in PSC frequency with a persistent current lasting >3 s (ref. 27). The duration, mean persistent current amplitude and mean charge transfer rate of PSC bursts were determined with Clampfit. The frequency and amplitude of spontaneous PSCs were quantified using MiniAnalysis (Synaptosoft, Inc., Decatur, GA, USA) with the detection threshold set at 10 pA for initial automatic event detection, followed by visual inspections to include missed events (≥ 5 pA) and to exclude false events resulting from baseline fluctuations. The software was set to search for a baseline 3 ms before a PSC event and use the average of a 1-ms period as the baseline level. Peak amplitudes of evoked PSCs and of muscle responses to exogenous ACh or GABA were quantified using Clampfit. The average of the largest two evoked PSCs recorded from each muscle cell was used for statistical comparisons. Upstate was defined as a sudden increase (>5 mV) in the membrane potential lasting longer than 3 s. Upstate potential was the mean membrane voltage during the upstate (quantified with Clampfit), whereas upstate amplitude was the voltage difference between upstate potential and the resting membrane potential. All the upstates of each recording (3–5 min) were analysed to obtain an averaged value of each parameter (for example, amplitude and duration) before statistical analyses. Statistical comparisons were performed with OriginPro (version 9, OriginLab, Northampton, MA, USA) using either one-way analyses of variance or unpaired *t*-test (depending on whether there were >2 groups). All values are shown as mean ± s.e. $P<0.05$ is considered to be statistically significant. The sample size (n) equals the number of cells or membrane patches analysed. Data graphing was performed with OriginPro.

References

1. Trussell, L. O. & Roberts, M. T. in *Molecular Mechanisms of Neurotransmitter Release* (ed. Wang, Z. W.) (Humana Press, 2008).
2. Bhattacharjee, A., Gan, L. & Kaczmarek, L. K. Localization of the Slack potassium channel in the rat central nervous system. *J. Comp. Neurol.* **454,** 241–254 (2002).
3. Bhattacharjee, A., von Hehn, C. A., Mei, X. & Kaczmarek, L. K. Localization of the Na^+-activated K^+ channel Slick in the rat central nervous system. *J. Comp. Neurol.* **484,** 80–92 (2005).
4. Hage, T. A. & Salkoff, L. Sodium-activated potassium channels are functionally coupled to persistent sodium currents. *J. Neurosci.* **32,** 2714–2721 (2012).
5. Budelli, G. *et al.* Na^+-activated K^+ channels express a large delayed outward current in neurons during normal physiology. *Nat. Neurosci.* **12,** 745–750 (2009).
6. Lu, S., Das, P., Fadool, D. A. & Kaczmarek, L. K. The slack sodium-activated potassium channel provides a major outward current in olfactory neurons of Kv1.3-/- super-smeller mice. *J. Neurophysiol.* **103,** 3311–3319 (2010).
7. Huang, F. *et al.* TMEM16C facilitates Na^+-activated K^+ currents in rat sensory neurons and regulates pain processing. *Nat. Neurosci.* **16,** 1284–1290 (2013).
8. Nuwer, M. O., Picchione, K. E. & Bhattacharjee, A. PKA-induced internalization of slack KNa channels produces dorsal root ganglion neuron hyperexcitability. *J. Neurosci.* **30,** 14165–14172 (2010).
9. Zhang, Y. *et al.* Regulation of neuronal excitability by interaction of fragile x mental retardation protein with slack potassium channels. *J. Neurosci.* **32,** 15318–15327 (2012).
10. Barcia, G. *et al. De novo* gain-of-function *KCNT1* channel mutations cause malignant migrating partial seizures of infancy. *Nat. Genet.* **44,** 1255–1259 (2012).
11. Heron, S. E. *et al.* Missense mutations in the sodium-gated potassium channel gene *KCNT1* cause severe autosomal dominant nocturnal frontal lobe epilepsy. *Nat. Genet.* **44,** 1188–1190 (2012).
12. Vanderver, A. *et al.* Identification of a novel *de novo* p.Phe932Ile *KCNT1* mutation in a patient with leukoencephalopathy and severe epilepsy. *Pediatr. Neurol.* **50,** 112–114 (2014).
13. Ishii, A. *et al.* A recurrent *KCNT1* mutation in two sporadic cases with malignant migrating partial seizures in infancy. *Gene* **531,** 467–471 (2013).
14. Dhamija, R., Wirrell, E., Falcao, G., Kirmani, S. & Wong-Kisiel, L. C. Novel *de novo SCN2A* mutation in a child with migrating focal seizures of infancy. *Pediatr. Neurol.* **49,** 486–488 (2013).
15. Yuan, A. *et al.* The sodium-activated potassium channel is encoded by a member of the *Slo* gene family. *Neuron* **37,** 765–773 (2003).
16. Bhattacharjee, A. *et al.* Slick (Slo2.1), a rapidly-gating sodium-activated potassium channel inhibited by ATP. *J. Neurosci.* **23,** 11681–11691 (2003).
17. Dryer, S. E. Molecular identification of the Na^+-activated K^+ channel. *Neuron* **37,** 727–728 (2003).
18. Kaczmarek, L. K. Slack, slick and sodium-activated potassium channels. *ISRN Neurosci.* **2013** pii 354262 (2013).
19. Bhattacharjee, A. & Kaczmarek, L. K. For K^+ channels, Na^+ is the new Ca^{2+}. *Trends Neurosci.* **28,** 422–428 (2005).
20. Wallen, P. *et al.* Sodium-dependent potassium channels of a Slack-like subtype contribute to the slow afterhyperpolarization in lamprey spinal neurons. *J. Physiol.* **585,** 75–90 (2007).
21. Yang, B., Desai, R. & Kaczmarek, L. K. Slack and Slick K_{Na} channels regulate the accuracy of timing of auditory neurons. *J. Neurosci.* **27,** 2617–2627 (2007).
22. Nanou, E. *et al.* Na^+-mediated coupling between AMPA receptors and K_{Na} channels shapes synaptic transmission. *Proc. Natl Acad. Sci. USA* **105,** 20941–20946 (2008).
23. Yuan, A. *et al.* SLO-2, a K^+ channel with an unusual Cl^- dependence. *Nat. Neurosci.* **3,** 771–779 (2000).
24. Salkoff, L., Butler, A., Ferreira, G., Santi, C. & Wei, A. High-conductance potassium channels of the SLO family. *Nat. Rev. Neurosci.* **7,** 921–931 (2006).
25. Liu, P. *et al.* Genetic dissection of ion currents underlying all-or-none action potentials in *C. elegans* body-wall muscle cells. *J. Physiol.* **589,** 101–117 (2011).
26. Lim, H. H. *et al.* Identification and characterization of a putative *C. elegans* potassium channel gene (*Ce-slo-2*) distantly related to Ca^{2+}-activated K^+ channels. *Gene* **240,** 35–43 (1999).
27. Liu, P., Chen, B. & Wang, Z. W. Postsynaptic current bursts instruct action potential firing at a graded synapse. *Nat. Commun.* **4,** 1911 (2013).
28. de Bono, M. & Maricq, A. V. Neuronal substrates of complex behaviors in *C. elegans*. *Annu. Rev. Neurosci.* **28,** 451–501 (2005).
29. Chalfie, M. & White, J. in *The Nematode Caenorhabditis elegans.* (ed. Wood, W. B., Researchers TCoCe) (Cold Spring Harbor Laboratory Press, 1988).
30. Wei, A. *et al.* Efficient isolation of targeted Caenorhabditis elegans deletion strains using highly thermostable restriction endonucleases and PCR. *Nucleic Acids Res.* **30,** e110 (2002).
31. Mahoney, T. R. *et al.* Regulation of synaptic transmission by RAB-3 and RAB-27 in Caenorhabditis elegans. *Mol. Biol. Cell.* **17,** 2617–2625 (2006).
32. Nonet, M. L. *et al.* Caenorhabditis elegans rab-3 mutant synapses exhibit impaired function and are partially depleted of vesicles. *J. Neurosci.* **17,** 8061–8073 (1997).
33. Salkoff, L. *et al.* in *WormBook* (ed. The *C. elegans* Research Community) doi:doi/10.1895/wormbook.1.42.1 (2005).
34. Santi, C. M. *et al.* Dissection of K^+ currents in *Caenorhabditis elegans* muscle cells by genetics and RNA interference. *Proc. Natl Acad. Sci. USA* **100,** 14391–14396 (2003).
35. Fawcett, G. L. *et al.* Mutant analysis of the Shal (Kv4) voltage-gated fast transient K^+ channel in *Caenorhabditis elegans*. *J. Biol. Chem.* **281,** 30725–30735 (2006).
36. Wang, Z. W., Saifee, O., Nonet, M. L. & Salkoff, L. SLO-1 potassium channels control quantal content of neurotransmitter release at the *C. elegans* neuromuscular junction. *Neuron* **32,** 867–881 (2001).
37. Liu, Q., Chen, B., Ge, Q. & Wang, Z. W. Presynaptic Ca^{2+}/calmodulin-dependent protein kinase II modulates neurotransmitter release by activating BK channels at *Caenorhabditis elegans* neuromuscular junction. *J. Neurosci.* **27,** 10404–10413 (2007).
38. Zhang, Z. *et al.* SLO-2 isoforms with unique Ca^{2+}- and voltage-dependence characteristics confer sensitivity to hypoxia in *C. elegans*. *Channels (Austin)* **7,** 194–205 (2013).

39. Bargmann, C. I. Neurobiology of the *Caenorhabditis elegans* genome. *Science* **282,** 2028–2033 (1998).
40. Bauer Huang, S. L. *et al.* Left-right olfactory asymmetry results from antagonistic functions of voltage-activated calcium channels and the Raw repeat protein OLRN-1 in *C. elegans*. *Neural. Dev.* **2,** 24 (2007).
41. Steger, K. A., Shtonda, B. B., Thacker, C., Snutch, T. P. & Avery, L. The *C. elegans* T-type calcium channel CCA-1 boosts neuromuscular transmission. *J. Exp. Biol.* **208,** 2191–2203 (2005).
42. Lee, R. Y., Lobel, L., Hengartner, M., Horvitz, H. R. & Avery, L. Mutations in the α1 subunit of an L-type voltage-activated Ca^{2+} channel cause myotonia in *Caenorhabditis elegans*. *EMBO J.* **16,** 6066–6076 (1997).
43. Feng, Z. *et al.* A *C. elegans* model of nicotine-dependent behavior: regulation by TRP-family channels. *Cell* **127,** 621–633 (2006).
44. Tanis, J. E. *et al.* CLHM-1 is a functionally conserved and conditionally toxic Ca^{2+}-permeable ion channel in *Caenorhabditis elegans*. *J. Neurosci.* **33,** 12275–12286 (2013).
45. Yeh, E. *et al.* A putative cation channel, NCA-1, and a novel protein, UNC-80, transmit neuronal activity in *C. elegans*. *PLoS Biol.* **6,** e55 (2008).
46. Jospin, M. *et al.* UNC-80 and the NCA ion channels contribute to endocytosis defects in synaptojanin mutants. *Curr. Biol.* **17,** 1595–1600 (2007).
47. Maryon, E. B., Coronado, R. & Anderson, P. *unc-68* encodes a ryanodine receptor involved in regulating *C. elegans* body-wall muscle contraction. *J. Cell Biol.* **134,** 885–893 (1996).
48. Liu, Q. *et al.* Presynaptic ryanodine receptors are required for normal quantal size at the *Caenorhabditis elegans* neuromuscular junction. *J. Neurosci.* **25,** 6745–6754 (2005).
49. Hyde, R., Corkins, M. E., Somers, G. A. & Hart, A. C. PKC-1 acts with the ERK MAPK signaling pathway to regulate Caenorhabditis elegans mechanosensory response. *Genes Brain Behav.* **10,** 286–298 (2011).
50. Glauser, D. A. *et al.* Heat avoidance is regulated by transient receptor potential (TRP) channels and a neuropeptide signaling pathway in *Caenorhabditis elegans*. *Genetics* **188,** 91–103 (2011).
51. Humphrey, J. A. *et al.* A putative cation channel and its novel regulator: cross-species conservation of effects on general anesthesia. *Curr. Biol.* **17,** 624–629 (2007).
52. Enyedi, P. & Czirjak, G. Molecular background of leak K^+ currents: two-pore domain potassium channels. *Physiol. Rev.* **90,** 559–605 (2010).
53. Chen, B., Liu, P., Zhan, H. & Wang, Z. W. Dystrobrevin controls neurotransmitter release and muscle Ca^{2+} transients by localizing BK channels in *Caenorhabditis elegans*. *J. Neurosci.* **31,** 17338–17347 (2011).
54. Saheki, Y. & Bargmann, C. I. Presynaptic CaV2 calcium channel traffic requires CALF-1 and the $\alpha_2\delta$ subunit UNC-36. *Nat. Neurosci.* **12,** 1257–1265 (2009).
55. Davies, A. G. *et al.* A central role of the BK potassium channel in behavioral responses to ethanol in *C. elegans*. *Cell* **115,** 655–666 (2003).
56. Chen, B. *et al.* A novel auxiliary subunit critical to BK channel function in *Caenorhabditis elegans*. *J. Neurosci.* **30,** 16651–16661 (2010).
57. Kim, H. *et al.* The dystrophin complex controls bk channel localization and muscle activity in *Caenorhabditis elegans*. *PLoS Genet.* **5,** e1000780 (2009).
58. Carre-Pierrat, M. *et al.* The SLO-1 BK channel of *Caenorhabditis elegans* is critical for muscle function and is involved in dystrophin-dependent muscle dystrophy. *J. Mol. Biol.* **358,** 387–395 (2006).
59. Abraham, L. S., Oh, H. J., Sancar, F., Richmond, J. E. & Kim, H. An alpha-catulin homologue controls neuromuscular function through localization of the dystrophin complex and BK channels in *Caenorhabditis elegans*. *PLoS Genet.* **6** pii e1001077 (2010).
60. Chen, B. *et al.* **α**-Catulin CTN-1 is required for BK channel subcellular localization in *C. elegans* body-wall muscle cells. *EMBO J.* **29,** 3184–3195 (2010).
61. Jegla, T. J., Zmasek, C. M., Batalov, S. & Nayak, S. K. Evolution of the human ion channel set. *Comb. Chem. High. Throughput. Screen.* **12,** 2–23 (2009).
62. Evans, T. in *WormBook* (ed. The *C. elegans* Research Community) doi:doi/10.1895/wormbook.1.108.1 (2006).
63. White, J. G., Southgate, E., Thomson, J. N. & Brenner, S. The structure of the nervous system of the nematode *Caenorhabditis elegans*. *Philos. Trans. R. Soc. Lond. B Biol. Sci.* **314,** 1–340 (1986).

Acknowledgements

This work was supported by National Institute of Health (1R01MH085927, to Z.-W.W.). We thank Caenorhabditis Genetics Center (USA), Erik Jorgensen laboratory and Lawrence Salkoff laboratory for providing mutant strains.

Author contributions

P.L. and Z.-W.W. conceived the project; P.L. and B.C. performed the experiments; and Z.-W.W. and P.L. wrote the manuscript.

Additional information

Competing financial interests: The authors declare no competing financial interests.

Reprints and permission information is available online at http://npg.nature.com/reprintsandpermissions/

How to cite this article: Liu, P. *et al.* SLO-2 potassium channel is an important regulator of neurotransmitter release in *Caenorhabditis elegans*. *Nat. Commun.* 5:5155 doi: 10.1038/ncomms6155 (2014).